Programmable motion of DNA origami mechanisms

Alexander E. Marras, Lifeng Zhou, Hai-Jun Su, and Carlos E. Castro[1]

Department of Mechanical and Aerospace Engineering, The Ohio State University, Columbus, OH 43210

Edited by William Shih, Harvard University, Cambridge, MA, and accepted by the Editorial Board December 10, 2014 (received for review May 13, 2014)

DNA origami enables the precise fabrication of nanoscale geometries. We demonstrate an approach to engineer complex and reversible motion of nanoscale DNA origami machine elements. We first design, fabricate, and characterize the mechanical behavior of flexible DNA origami rotational and linear joints that integrate stiff double-stranded DNA components and flexible single-stranded DNA components to constrain motion along a single degree of freedom and demonstrate the ability to tune the flexibility and range of motion. Multiple joints with simple 1D motion were then integrated into higher order mechanisms. One mechanism is a crank–slider that couples rotational and linear motion, and the other is a Bennett linkage that moves between a compacted bundle and an expanded frame configuration with a constrained 3D motion path. Finally, we demonstrate distributed actuation of the linkage using DNA input strands to achieve reversible conformational changes of the entire structure on ∼minute timescales. Our results demonstrate programmable motion of 2D and 3D DNA origami mechanisms constructed following a macroscopic machine design approach.

DNA nanotechnology | DNA origami | dynamic structures | machine design | self-assembly

The ability to control, manipulate, and organize matter at the nanoscale has demonstrated immense potential for advancements in industrial technology, medicine, and materials (1–3). Bottom-up self-assembly has become a particularly promising area for nanofabrication (4, 5); however, to date designing complex motion at the nanoscale remains a challenge (6–9). Amino acid polymers exhibit well-defined and complex dynamics in natural systems and have been assembled into designed structures including nanotubes, sheets, and networks (10–12), although the complexity of interactions that govern amino acid folding make designing complex geometries extremely challenging. DNA nanotechnology, on the other hand, has exploited well-understood assembly properties of DNA to create a variety of increasingly complex designed nanostructures (13–15).

Scaffolded DNA origami, the process of folding a long single-stranded DNA (ssDNA) strand into a custom structure (16–18), has enabled the fabrication of nanoscale objects with unprecedented geometric complexity that have recently been implemented in applications such as containers for drug delivery (19, 20), nanopores for single-molecule sensing (21–23), and templates for nanoparticles (24, 25) or proteins (26–28). The majority of these and other applications of DNA origami have largely focused on static structures. Natural biomolecular machines, in contrast, have a rich diversity of functionalities that rely on complex but well-defined and reversible conformational changes. Currently, the scope of biomolecular nanotechnology is limited by an inability to achieve similar motion in designed nanosystems.

DNA nanotechnology has enabled critical steps toward that goal starting with the work of Mao et al. (29), who developed a DNA nanostructure that took advantage of the B–Z transition of DNA to switch states. Since then, efforts to fabricate dynamic DNA systems have primarily focused on strand displacement approaches (30) mainly on systems comprising a few strands or arrays of strands undergoing ∼nm-scale motions (31–37) in some cases guided by DNA origami templates (38–40). More recently, strand displacement has been used to reconfigure DNA origami nanostructures, for example opening DNA containers (19, 41, 42), controlling molecular binding (43, 44), or reconfiguring structures (45). The largest triggerable structural change was achieved by Han et al. in a DNA origami Möbius strip (one-sided ribbon structure) that could be opened to approximately double in size (45). Constrained motion has been achieved in systems with rotational motion (19, 20, 32, 41, 44, 46, 47) in some cases to open lid-like components (19, 20, 41) or detect molecular binding (44, 48, 49). A few of these systems achieved reversible conformational changes (32, 41, 44, 46), although the motion path and flexibility were not studied. Constrained linear motion has remained largely unexplored. Linear displacements on the scale of a few nanometers have been demonstrated via conformational changes of DNA structure motifs (50–55), strand invasion to open DNA hairpins (36, 55, 56), or the reversible sliding motion of a DNA tile actuator (56); these cases also did not investigate the motion path or flexibility of motion.

Building on these prior studies, this work implements concepts from macroscopic machine design to build modular parts with constrained motion. We demonstrate an ability to tune the flexibility and range of motion and then integrate these parts into prototype mechanisms with designed 2D and 3D motion. We further demonstrate reversible actuation of a mechanism with complex conformational changes on minute timescales.

DNA Origami Mechanism Design

A kinematic mechanism is a mechanical device that transforms an input motion from an actuator to a defined motion pattern (57). They typically comprise a collection of interconnected components called links whose motion is constrained by so-called kinematic joints, such as revolute (hinge), prismatic (slider), and spherical joints. Complex 3D motion is achieved by integrating multiple joints with precisely designed geometric components into a mechanism. In nanoscale design, specific mechanical motion has seldom been explored. Whereas rotational (19, 20, 32, 41, 44, 46–49) and small linear motions (36, 50–56) have been demonstrated, the mechanics of this motion have not been studied in any detail. Here we use scaffolded DNA origami to integrate stiff double-stranded DNA (dsDNA) and

Significance

Folding DNA into complex 3D shapes (DNA origami) has emerged as a powerful method for the precise design and fabrication of self-assembled nanodevices. Current efforts have focused largely on developing static objects or structures with small movements and/or unspecified motion paths. Here we establish a basis for developing DNA-based nanomachines by creating dynamic mechanisms with well-defined motion. We demonstrate the design of nanoscale 1D, 2D, and 3D motion by integrating concepts from engineering machine design with DNA origami nanotechnology.

Author contributions: A.E.M., L.Z., H.-J.S., and C.E.C. designed research; A.E.M. and L.Z. performed research; A.E.M., H.-J.S., and C.E.C. analyzed data; and A.E.M. and C.E.C. wrote the paper.

The authors declare no conflict of interest.

This article is a PNAS Direct Submission. W.S. is a guest editor invited by the Editorial Board.

[1]To whom correspondence should be addressed. Email: castro.39@osu.edu.

This article contains supporting information online at www.pnas.org/lookup/suppl/doi:10.1073/pnas.1408869112/-/DCSupplemental.

flexible ssDNA components to create mechanical devices capable of precise motion over ∼10–100-nm range.

Our design approach, which parallels macroscopic mechanism design, is conceptualized in Fig. 1 with an example of a mechanism that couples rotational and linear motion. In macroscopic machines, joints are typically designed by combining stiff components along an edge (e.g., hinge; Fig. 1, *Top*) or with complementary geometry (e.g., slider; Fig. 1, *Middle*). In DNA origami, similar functionality can be achieved either by strategic placement of flexible ssDNA connections (e.g., along a line to form a hinge axis) or complementary geometry (e.g., concentric structures). These joints can be combined to create higher order mechanisms (e.g., crank–slider; Fig. 1, *Bottom*) with complex predefined motion. We focus on slider and hinge joints and their implementation into mechanisms with controllable motion.

DNA Nanostructures for Simple Motion

A DNA origami slider joint was created to produce linear motion by connecting two stiff bundles with complementary geometry using flexible ssDNA scaffold connections as depicted in Fig. 2. The two components are self-assembled concentrically, which to our knowledge has not previously been shown with DNA origami. The outer tube of 30 helices surrounds an inner 6-helix bundle (hb) with roughly 2 nm of clearance. At the base of the 6 hb is a 42 hb, which sterically limits the translation of the outer tube. Long ssDNA scaffold strands connect the outer tube and inner 6 hb to allow for relative linear motion (Fig. 2*A*).

We fabricated two versions of the slider (Fig. 2 *C* and *D*) with different ranges of motion and stiffness controlled by varying the length of the ssDNA scaffold connections. Version 1 has six 49-nucleotide (nt) connections between the 30-hb tube and 42-hb base and six 28-nt connections between the 30-hb tube and inner 6 hb at the opposite end. Six 15-nt staples were added to prevent hairpins in the 49-nt connections (Fig. S1). Thermal fluctuations cause the joint to extend and contract along the linear motion path. The extensional distribution (Fig. 2*B*), measured by transmission electron microscopy (TEM), revealed a range of thermal motion of 14.0 nm. The second version, with a larger range of motion, has 86-nt connections between the tube and base and 96-nt connections between the tube and the end of the 6 hb. Three 18–20-nt staples were added to each connection to prevent hairpins (Fig. S1). This design resulted in a range of motion of 29.2 nm (extensional distribution shown in Fig. 2*D*). The energy landscape for both designs was determined from extensional measurements assuming a Boltzmann distribution (details in *SI Text*). The mechanics of motion are likely mediated largely by the entropic elasticity and steric effects of the ssDNA connections. Extension of the ssDNA lowers their entropy, resulting in higher energy, or equivalently lower probability, conformations. Whereas electrostatic interactions between the tube and inner 6 hb would not change as the joint moves, electrostatic interactions between the tube and the base or between connections may provide additional resistance to extension or contraction. The force versus extension behavior of both joints was approximated by differentiating the energy landscape (Fig. 2*F*). The first design (shorter connections) resembles a linear spring with a stiffness of 0.42 pN/nm, whereas the longer (and fewer) connections resulted in nonlinear force-extension behavior with a stiffness of 0.07 pN/nm at smaller extensions and 0.21 pN/nm for longer extensions, with the transition occurring at the equilibrium (zero-force) position. Using fewer and longer ssDNA connections (version 2) resulted in a larger range of motion; however, these factors also occasionally caused the outer tube to fold apart from the inner 6 hb, instead of forming concentrically (Fig. S2). Misfolded structures were omitted from the motion analysis. These DNA origami slider joints demonstrate the ability to design constrained linear motion with tunable flexibility.

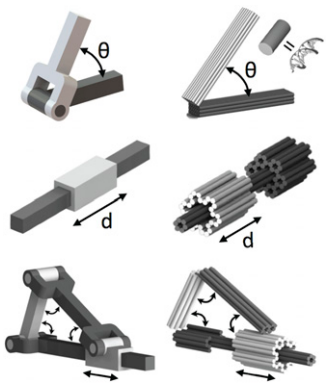

Fig. 1. DNA origami mechanism design. Our approach to DNA origami mechanism design follows macroscopic machine design starting with isolated joints for angular (*Top*) or linear (*Middle*) motion. Joints can be integrated to achieve complex motion as shown here for a crank–slider mechanism (*Bottom*). *Left* shows macroscale solid models and *Right* shows their DNA origami counterparts. In the DNA origami designs, cylinders represent dsDNA helices.

Rotational and linear motion can be combined to create any complex motion. With this in mind, we also created a device constrained to purely rotational motion. Our DNA origami revolute joint, or hinge, consists of two stiff arms (18 hb, 3 × 6 square lattice) joined along an edge by flexible ssDNA scaffold connections made along a line that defines the hinge axis (Fig. 3*A*). On three of the helices where hinge connections are made, the scaffold is at an appropriate helical position to make short connections. These ssDNA connections are 2 nt in all cases. On the other three helices, the scaffold is at the opposing helical position and the connections must traverse the diameter of both helices. Two versions of the hinge were designed where the length of these connections was 16 (hinge 1) and 30 (hinge 2) nt, respectively. The short connections define the hinge axis, and the long connections influence the motion due to entropic elasticity, electrostatic interactions, and steric effects. Two 12-nt strands were added to cover secondary structure on each of the three long connections of hinge 2 to ensure flexible rotation (Fig. S1). The two lower rows of helices on the bottom arm provide a physical constraint at the back of the joint that prevents full opening of the arms (Fig. S1).

Fig. 3*A* depicts a zoomed-in TEM image of the revolute joint compared with the design model, and Fig. 3*B* shows a distribution of conformations of hinge 2 in a representative TEM image. Additional TEM images of both hinges are available in Fig. S2. Joint angles varied from 11° to 147° with an average of 79.7° for hinge 1. Hinge 2 exhibited a range of 11–131° with an average of 62°. Movie S1 shows several TEM snapshots of samples at different configurations sequentially ordered to visualize the observed range of angles of hinge 2. TEM generally revealed hinges lying on their side. A few hinges were observed in the perpendicular orientation (top or bottom view) and revealed there was little out-of-plane rotation (Fig. S2). The energy landscapes of the hinges (Fig. 3*E*) were similarly determined assuming a Boltzmann distribution, and the torques (Fig. 3*F*) required to hold the hinges at any specific angle were calculated by differentiating the energy landscape (details in *SI Text*).

Hinge 1 behaves approximately like a linear torsional spring with a stiffness (slope in Fig. 3*F*) of 25 pN-nm/rad that increases to 45 pN-nm/rad at angles $\gtrsim$100° or $\lesssim$40°. Hinge 2 behaves like a nonlinear torsional spring with a stiffness of ∼70 pN-nm/rad at $\lesssim$40° and $\gtrsim$80° with flexible rotation in the range between. The rotational flexibility is likely dominated by electrostatic interactions between the arms and entropic elasticity and steric effects of the ssDNA connections at the hinge. Interestingly, for hinge 2, the torsional stiffness at small and large angles is similar to the stiffness of natural proteins that function as cross-linking components, such as the actin binding protein Arp 2/3 (∼80–130 pN-nm/rad) (58).

DNA Nanostructures for Complex Motion

Stiff components and flexible joints can be integrated into functional mechanisms where motion is determined by the geometry

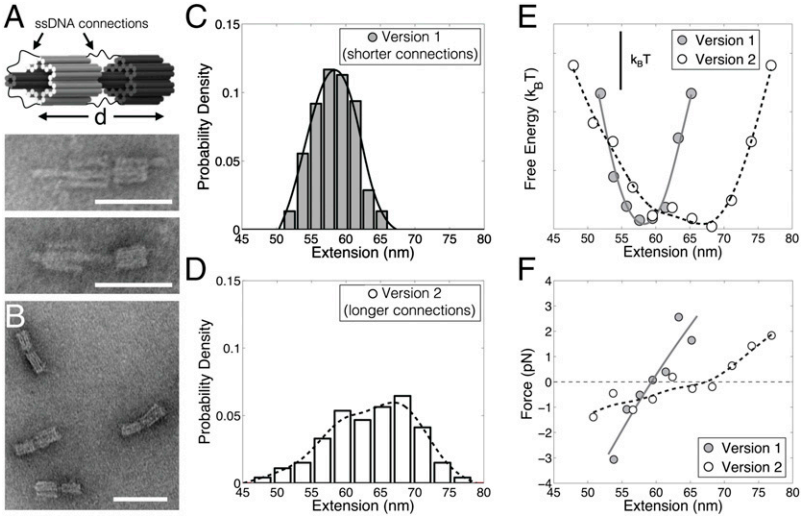

Fig. 2. DNA origami sliders. (*A*) The slider consists of two stiff components folded concentrically and connected only with ssDNA scaffold facilitating linear motion. Two versions of the slider were fabricated, one with short ssDNA connections (version 1) and one with long ssDNA connections (version 2). TEM images illustrate different conformations of version 2. Scale bar, 50 nm (*B*) Version 1 (shorter connections) is shown via TEM. Scale bar, 100 nm (*C*) A linear distribution of 14 nm was measured from 275 samples of version 1. (*D*) A wider linear distribution was measured from 251 samples of version 2. (*E*) The energy landscape was calculated for both versions from the linear distributions assuming Boltzmann energy weighting (scale bar indicates an energy scale of k_BT). The lines show cubic spline fits to linear distributions. (*F*) The energy landscape was differentiated to determine the force required to hold each joint at any specific length.

of the stiff components and the arrangement and degrees of freedom of the joints. We designed two DNA origami mechanisms that integrate multiple joints to achieve 2D and 3D complex motion. Fig. 4 *A* and *B* show a model and TEM images of a DNA origami mechanism known as a crank–slider that combines three hinges and one slider joint. This mechanism is geometrically constrained to one degree of freedom and couples rotational and linear motion in 2D. The joints in this mechanism closely follow the hinge and slider designs discussed above. The hinges comprise two 2-nt-long ssDNA scaffold connections to define the hinge axis and two 34-nt connections on the neighboring helices. The long connections each have two 12-nt staples to cover hairpin locations. The slider has two 52-nt connections between the tube and the base and two 77-nt connections between the tube and the end of the 6 hb, each with two 16–20-nt staples to prevent hairpins (full design details in Fig. S3). The relationship between angular and linear motion is depicted in Fig. 4*C* with the theoretical relation (derivation in Fig. S4) shown in black. The gray "x"s represent the conformation of individual DNA origami crank–sliders measured from TEM images. These closely follow the theoretical prediction with some fluctuations, likely due to extra flexibility in the DNA links and joints. Only well-folded structures were included in the analysis.

The second mechanism consists of four hinges and four 16-hb (4 × 4 square arrangement) links. The hinges were formed with two 2-nt connections defining the hinge axes. The mechanism, called a Bennett linkage (59), exhibits a well-defined 3D motion path with two extreme conformations: an open frame and a compact bundle (Fig. 5*A*). In particular, we fabricated the "alternative" form of a Bennett linkage, where all four links have the same length (60). Complete design details are provided in *SI Text* (Fig. S3). This type of mechanism is used in macroscopic systems as an expandable device for packaging or deployment (61). It can also be combined in a lattice of identical linkages to perform larger conformational changes (62).

TEM images of the Bennett linkage (Fig. 5*B*) indicate that the mechanism explores the full motion path ranging from the bundle to the expanded frame. Only a small fraction of the mechanisms was observed in the closed bundle configuration, likely due to electrostatic repulsions. To confirm the range of motion, mechanisms were fixed in the extreme conformations (Fig. 5*D*, expanded frame and Fig. 5*E*, compacted bundle) by incorporating additional ssDNA staples (Fig. S5). Eighty-one percent of the linkages were successfully held in the expanded configuration and 93% in the compacted configuration. These results represent upper bounds because surface deposition may force nearly expanded or nearly compacted mechanisms into their respective extreme configuration. Additional TEM images of the unconstrained and constrained Bennett linkages are available in Fig. S6.

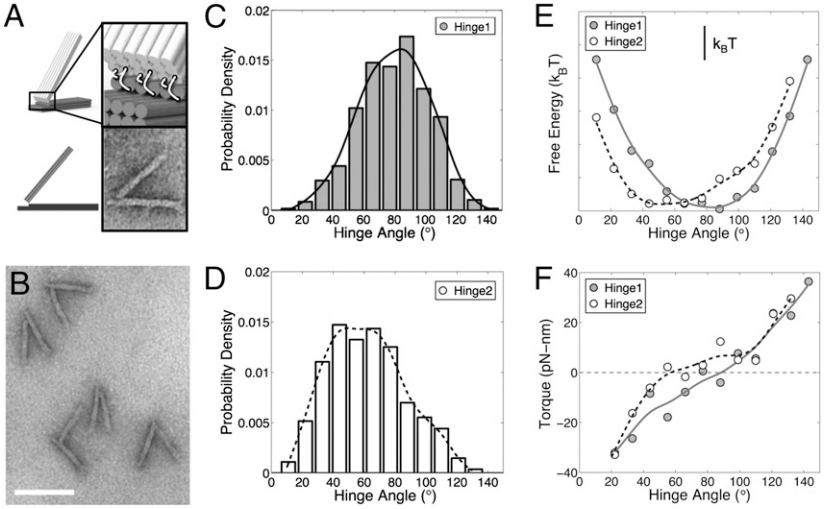

Fig. 3. DNA origami hinges. (*A*) The hinge consists of two stiff bundles of 18 dsDNA helices connected at one end by 6 ssDNA connections (white lines). Two versions of the hinge were fabricated. The short connections are 2 nt long in both designs and the long connections are 16 and 30 nt for hinge 1 and hinge 2, respectively. (*B*) TEM images of hinge 2 confirm well-folded structures and flexible motion in one angular degree of freedom. Scale bar, 100 nm. (*C*) The angular distribution of hinge 1, measured from 918 structures in TEM images, shows a torsionally stiff joint with an equilibrium angle of ~85°. (*D*) The angular distribution of hinge 2, measured from 248 structures in TEM images, shows resistance to small (<40°) and large (>80°) angles with relative flexibility in the range between. (*E*) The energy landscape was calculated from the angular distributions assuming Boltzmann energy weighting (scale bar indicates an energy scale of k_BT). The lines show cubic spline fits to angular distributions. (*F*) The energy landscape was differentiated to determine the torque required to hold each hinge at any specific angle.

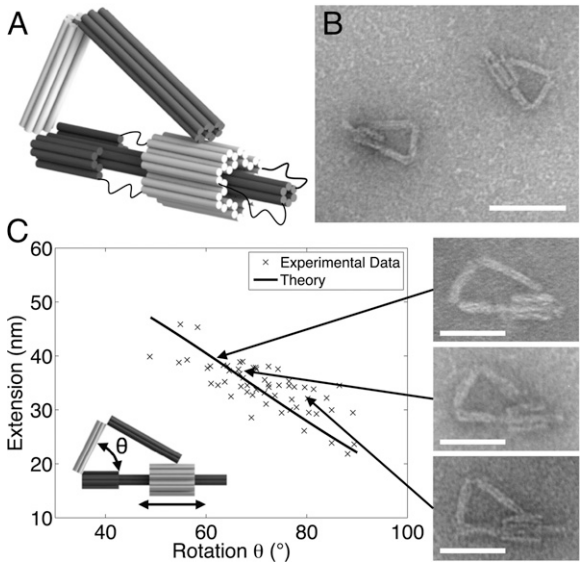

Fig. 4. DNA origami crank–slider coupling linear and rotational motion. (*A*) The mechanism incorporates three hinges and one slider joint using designs from Figs. 2 and 3 to achieve 2D motion. (*B*) TEM shows samples of the mechanisms. Scale bar, 100 nm. (*C*) The motion of the DNA origami crank–slider, illustrated by measurements of rotation vs. extension from TEM images for 56 samples (gray "x"s), follows the theoretical prediction (black line) for its rigid-body counterpart with some fluctuation about the ideally constrained motion path. TEM images on the right depict zoomed-in views of crank–sliders in different configurations along the motion path. Scale bar, 50 nm.

In theory, Bennett linkages follow a well-defined 3D motion path with a single degree of freedom. It is difficult to verify 3D motion by typical imaging methods such as TEM or atomic force microscopy (AFM), and methods to reconstruct 3D DNA origami from TEM (63) are more suitable for structures that maintain a static geometry. Because the Bennett linkage exhibits a wide range of conformations on the motion path, we developed an analytical approach called "projection kinematics" to validate the motion of the linkage.

When a 3D object is deposited on a TEM sample grid, one surface usually falls flat on the grid. For the Bennett linkages, two of the four members (gray and red or blue and green in Fig. 5*A*) form a planar surface, which we assumed lay flat on the grid. The other two may point partially in the direction normal to the surface. Links that point partially in the normal direction appear shorter in the TEM 2D projection. Because the full geometry and motion path are known, the 3D conformation can be inferred from the 2D projection by kinematic analysis. Fig. 5*C* shows the theoretical relation between the projected angles α' and β' compared with direct measurements from TEM images for several samples (details of projection kinematics in *SI Text*, Fig. S7).

The kinematic analysis assumes links are rigid and hinges are ideally constrained. DNA origami 4 hb have been found to exhibit persistence lengths of 740 nm (64), suggesting a 16-hb is essentially rigid at the length scale of the mechanism (each link is ~35 nm long). The ssDNA hinge connections, however, consist of 2 nt, meaning the hinge axes are not ideally constrained, and individual helices may fluctuate at the ends of the links, where hinges are located. Furthermore, surface deposition and staining may affect the configuration seen on the grid. Even with these effects, the DNA mechanism closely follows the projection kinematics prediction. For β' angles (Fig. 5*C*) <45° (where α' exhibits a large rapid change), the four links begin to overlap, and the projected angles can no longer be measured. Movie S2 illustrates general theoretical motion of a Bennett linkage. Movie S3 compares several TEM snapshots of the DNA origami mechanism to model snapshots in the same configuration. The TEM snapshots illustrate the most likely motion path based on the motion constraints, although there are fluctuations about the intended trajectory (Fig. 5*C*).

Actuation

The compacted configuration of the Bennett linkage is a higher energy state due to electrostatic repulsion, as suggested by the low percentage of unconstrained mechanisms found in the bundle configuration (Fig. 5*B*). Adopting this higher energy state requires performing work, and correspondingly generating a force. Liedl et al., Zhou et al., and Shu et al. demonstrated the ability to store mechanical energy or perform mechanical work in DNA nanostructures through tensegrity structures (65), bending compliant structures (66), and i-Motif quadruplex compaction (52), respectively. Here we perform mechanical work through a distributed actuation approach illustrated in Fig. 6*A* to trigger the conformational change into the higher energy state. This method expands on prior approaches (44, 48) by using a significantly larger

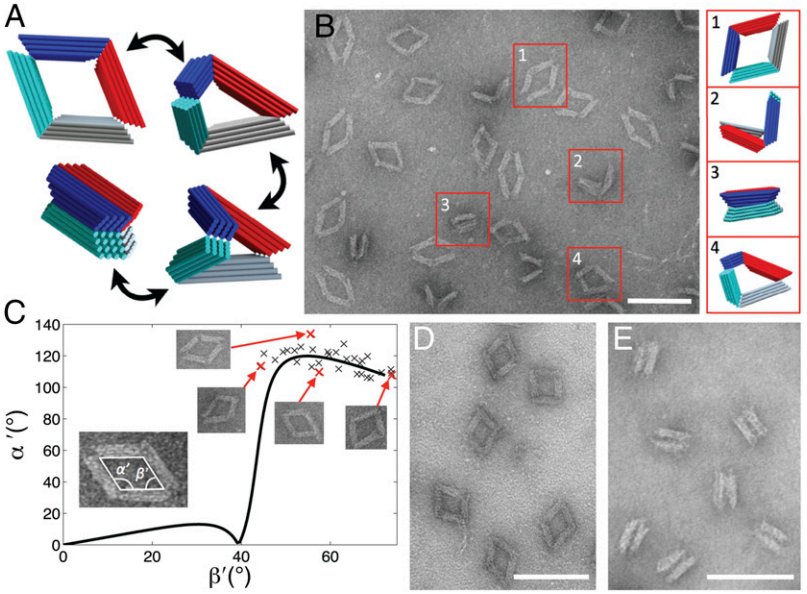

Fig. 5. DNA origami mechanism with 3D motion. (*A*) The four-bar mechanism called a Bennett linkage traverses a complex 3D motion path between extreme configurations of an open frame (*Top Left*) or a compacted bundle (*Bottom Left*). (*B*) TEM images confirm well-folded structures. In the absence of "locking strands" the mechanism fluctuates freely along its motion path. Several structures in different conformations are highlighted. (*C*) A comparison of the motion quantified in terms of the projected internal angles demonstrates that the DNA origami mechanism closely follows the expected motion path for its rigid-body counterpart (black line). Conformations were measured for 52 structures (gray "x"s) (*D*) Structures were fixed in their fully expanded frame configuration and (*E*) in their fully compacted bundle configuration. Scale bar, 100 nm.

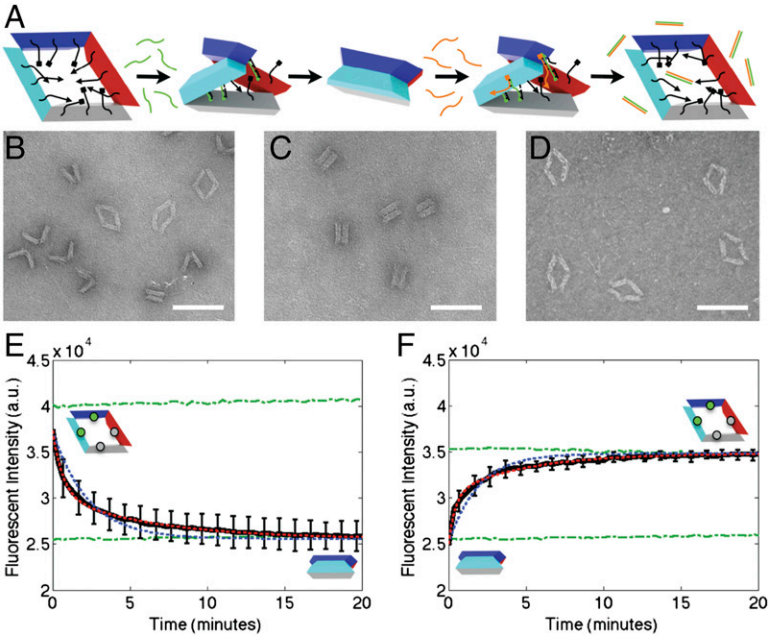

Fig. 6. Actuation of DNA origami mechanisms. (*A*) Distributed actuation was designed with several connections along the length of the links to zipper the mechanism into a higher energy compacted configuration. The compacted mechanisms can be expanded after a second addition of ssDNA inputs via strand displacement. (*B*) TEM images show the freely fluctuating configuration before actuation with input strands. In the free configuration 9.9% of mechanisms appear in the bundle conformation. (*C*) DNA origami mechanisms were actuated by adding twofold excess of closing strands that connect overhangs on different arms. After actuating the forward process (closing), 93% of mechanisms are found in the compacted bundle configuration on TEM images. (*D*) The reverse process (expanding) is achieved by a second set of DNA inputs that removes the closing strands by DNA strand displacement. (*E*) Fluorescence quenching data (black) reveal the timescale of compacting to be $t_{1/2,c} = 55$ s. (*F*) Expanding occurs on the timescale of $t_{1/2,e} = 49$ s. Single- (blue) and double- (red) exponential fits are shown as dashed lines. Unconstrained, compacted, and expanded controls are shown in green. The expanded control exhibits lower fluorescence because structures are diluted by addition of actuation strands. Scale bar, 100 nm.

number of actuation strand connections distributed throughout the structure to achieve cooperative binding. Sixty staples were designed to present ssDNA overhangs at corresponding locations on different links so that additional ssDNA inputs ("closing" strands) could bridge corresponding overhangs, forcing the mechanism into the bundled configuration. Overhangs were organized along the length of the links to allow "zippering" of the structure into the higher energy bundled state (Fig. S5). All overhangs on a single link comprised the same sequence so that multiple copies of the same closing strand could actuate the structure. Closing strands contained 5-nt toeholds to allow for their subsequent removal via toehold-mediated strand displacement (30, 31) similar to the actuation of the DNA origami Möbius strip (45). TEM images of the DNA origami Bennett linkage are shown in Fig. 6*B*, the unconstrained configuration; Fig. 6*C*, after the closing actuation; and Fig. 6*D*, after the opening actuation. The fraction of mechanisms that appeared bundled was 9.9% in the unconstrained case, 93.1% in the compacted structures, and 10.0% in the expanded structures, suggesting efficient actuation in both directions.

A fluorescence-quenching assay was used to monitor compaction and expansion of the mechanisms in real time. Fluorescent labels (Alexa488) and quenchers (Black Hole Quencher 1) were added to opposite arms (Fig. 6*E*, *Inset*) so that upon closing, fluorescence was quenched. Closing actuation occurred on a timescale of $t_{1/2,c} = 55$ s. Similarly, when the mechanism was expanded, fluorescence emission increased (Fig. 6*F*) on a timescale of $t_{1/2,e} = 49$ s. The expanding occurred faster than typical strand displacement reactions (67–69) perhaps because the process is accelerated by electrostatic repulsion driving toward a lower energy configuration. Both compacting and expansion exhibited double-exponential behavior (single- and double-exponential fits are shown in blue and red, respectively), which is consistent with previous actuation of DNA origami nanostructures (19).

The work presented here demonstrates the design, fabrication, and analysis of DNA origami joints and their incorporation into controllable mechanisms that can be actuated in a reversible fashion using DNA strand inputs on minute timescales. In particular, we demonstrated the ability to design 1D, 2D, and 3D motion that is constrained along a prescribed motion path. We also showed an ability to tune the flexibility of motion and conformational distribution of dynamic joints by modifying structure design parameters. This work lays the foundation for developing and characterizing a library of tunable DNA origami kinematic joints and using them in more complex controllable mechanisms similar to macroscopic machines, such as manipulators to control chemical reactions, transport biomolecules, or assemble nanoscale components in real time. Furthermore, the expandable mechanism presented here could serve as a basis for deployable nanosystems, actuators, or switchable devices in biosensing or triggered delivery applications.

Materials and Methods

Structures were designed in cadnano (70) and folded following protocols described in Castro et al. (18). In short, scaffold was mixed at 20 nM with 200 nM of each staple in a self-assembly reaction containing 1 mM EDTA, 5mM NaCl, 5 mM Tris, and 18–20 mM $MgCl_2$. Folding reactions were subjected to a thermal annealing ramp with initial heating to 65 °C to melt all interactions and then slow cooling to 25 °C over the timescale of 2 d. Well-folded structures were purified via 2% agarose gel electrophoresis (Fig. S8), and imaged by TEM for structure characterization (Figs. S2 and S6). TEM grids were prepared as described in Castro et al. (18) and imaged on an FEI Tecnai G2 Spirit TEM at an acceleration voltage of 80 kV. Staple sequences for all the structures presented are available in Dataset S1.

All DNA origami mechanisms were manually measured using the software ImageJ. The measurement error was characterized as 2.5° (SD) and 0.95 nm by making repeated measurements on the same structure (Fig. S9). Angular–linear distributions were created and motion analysis was performed in MATLAB.

Actuation experiments were performed on a Horiba Scientific Jobin Yvon Fluoromax-4 Spectrofluorometer using a 12-μL cuvette. Readings were taken before the addition of actuation strands to get a baseline fluorescence level. For the closing, actuation strands were added at twofold excess (110 nM) compared with the total number of connections on the mechanisms, and for opening, actuation strands were added at 20-fold excess compared with the closing strands (2 μM). The concentration of Bennett linkage structures after gel purification was measured to be 1.9 nM by UV absorbance on a Thermo Scientific NanoDrop 2000.

ACKNOWLEDGMENTS. We thank the Campus Microscopy and Imaging Facility and Center for Electron Microscopy and Analysis of The Ohio State University, and Dr. Michael Poirier from the Department of Physics of The Ohio State University for Spectrofluorometer access. This work was supported primarily by the National Science Foundation (NSF) under Grant CMMI-1235060. This work was also partially supported by the Center for Emergent Materials at The Ohio State University, an NSF Materials Research Science and Engineering Center (Award DMR-0820414).

1. Hamdi M, Ferreira A (2009) Multiscale design and modeling of protein-based nanomechanisms for nanorobotics. *Int J Robot Res* 28(4):436–449.
2. Mavroidis C, Dubey A, Yarmush ML (2004) Molecular machines. *Annu Rev Biomed Eng* 6(1):363–395.
3. Ummat ADA, Sharma G, Mavroidis C (2006) Bio-nanorobotics: State of the art and future challenges. *The Biomedical Engineering Handbook*, ed Yarmush ML (CRC Press, Boca Raton, FL).
4. Stephanopoulos N, Ortony JH, Stupp SI (2013) Self-assembly for the synthesis of functional biomaterials. *Acta Mater* 61(3):912–930.
5. Seeman NC (2010) Nanomaterials based on DNA. *Annu Rev Biochem* 79:65–87.
6. Chirikjian GS (2001) Conformational statistics of macromolecules using generalized convolution. *Comput Theor Polym Sci* 11(2):143–153.
7. Chirikjian GS, Kazerounian K, Mavroidis C (2005) Analysis and design of protein based nanodevices: Challenges and opportunities in mechanical design. *J Mech Des* 127(4):695–698.
8. Kazerounian K (2004) From mechanisms and robotics to protein conformation and drug design. *J Mech Des* 126(1):40–45.
9. Kazerounian K, Alvarado C, Latif K (2004) Protofold: A successive kinetostatic compliance method for protein conformation prediction. *J Mech Des* 127(4):712–717.
10. Chapman R, Danial M, Koh ML, Jolliffe KA, Perrier S (2012) Design and properties of functional nanotubes from the self-assembly of cyclic peptide templates. *Chem Soc Rev* 41(18):6023–6041.
11. Zhang S (2003) Fabrication of novel biomaterials through molecular self-assembly. *Nat Biotechnol* 21(10):1171–1178.
12. Matson JB, Zha RH, Stupp SI (2011) Peptide self-assembly for crafting functional biological materials. *Curr Opin Solid State Mater Sci* 15(6):225–235.
13. Seeman NC (1998) Nucleic acid nanostructures and topology. *Angew Chem Int Ed* 37(23):3220–3238.
14. Krishnan Y, Bathe M (2012) Designer nucleic acids to probe and program the cell. *Trends Cell Biol* 22(12):624–633.
15. Linko V, Dietz H (2013) The enabled state of DNA nanotechnology. *Curr Opin Biotechnol* 24(4):555–561.
16. Rothemund PW (2006) Folding DNA to create nanoscale shapes and patterns. *Nature* 440(7082):297–302.
17. Douglas SM, et al. (2009) Self-assembly of DNA into nanoscale three-dimensional shapes. *Nature* 459(7245):414–418.
18. Castro CE, et al. (2011) A primer to scaffolded DNA origami. *Nat Methods* 8(3): 221–229.
19. Andersen ES, et al. (2009) Self-assembly of a nanoscale DNA box with a controllable lid. *Nature* 459(7243):73–76.
20. Douglas SM, Bachelet I, Church GM (2012) A logic-gated nanorobot for targeted transport of molecular payloads. *Science* 335(6070):831–834.
21. Wei R, Martin TG, Rant U, Dietz H (2012) DNA origami gatekeepers for solid-state nanopores. *Angew Chem Int Ed Engl* 51(20):4864–4867.
22. Langecker M, et al. (2012) Synthetic lipid membrane channels formed by designed DNA nanostructures. *Science* 338(6109):932–936.
23. Bell NA, et al. (2012) DNA origami nanopores. *Nano Lett* 12(1):512–517.
24. Bui H, et al. (2010) Programmable periodicity of quantum dot arrays with DNA origami nanotubes. *Nano Lett* 10(9):3367–3372.
25. Ding B, et al. (2010) Gold nanoparticle self-similar chain structure organized by DNA origami. *J Am Chem Soc* 132(10):3248–3249.
26. Jungmann R, et al. (2011) DNA origami-based nanoribbons: Assembly, length distribution, and twist. *Nanotechnology* 22(27):275301.
27. Saccà B, et al. (2010) Orthogonal protein decoration of DNA origami. *Angew Chem Int Ed Engl* 49(49):9378–9383.
28. Derr ND, et al. (2012) Tug-of-war in motor protein ensembles revealed with a programmable DNA origami scaffold. *Science* 338(6107):662–665.
29. Mao C, Sun W, Shen Z, Seeman NC (1999) A nanomechanical device based on the B-Z transition of DNA. *Nature* 397(6715):144–146.
30. Zhang DY, Seelig G (2011) Dynamic DNA nanotechnology using strand-displacement reactions. *Nat Chem* 3(2):103–113.
31. Yurke B, Turberfield AJ, Mills AP, Jr, Simmel FC, Neumann JL (2000) A DNA-fuelled molecular machine made of DNA. *Nature* 406(6796):605–608.
32. Yan H, Zhang X, Shen Z, Seeman NC (2002) A robust DNA mechanical device controlled by hybridization topology. *Nature* 415(6867):62–65.
33. Yin P, Yan H, Daniell XG, Turberfield AJ, Reif JH (2004) A unidirectional DNA walker that moves autonomously along a track. *Angew Chem Int Ed Engl* 43(37):4906–4911.
34. Bishop JD, Klavins E (2007) An improved autonomous DNA nanomotor. *Nano Lett* 7(9):2574–2577.
35. Omabegho T, Sha R, Seeman NC (2009) A bipedal DNA Brownian motor with coordinated legs. *Science* 324(5923):67–71.
36. Feng L, Park SH, Reif JH, Yan H (2003) A two-state DNA lattice switched by DNA nanoactuator. *Angew Chem Int Ed Engl* 42(36):4342–4346.
37. Bath J, Turberfield AJ (2007) DNA nanomachines. *Nat Nanotechnol* 2(5):275–284.
38. Lund K, et al. (2010) Molecular robots guided by prescriptive landscapes. *Nature* 465(7295):206–210.
39. Zhang F, Nangreave J, Liu Y, Yan H (2012) Reconfigurable DNA origami to generate quasifractal patterns. *Nano Lett* 12(6):3290–3295.
40. Gu H, Chao J, Xiao SJ, Seeman NC (2010) A proximity-based programmable DNA nanoscale assembly line. *Nature* 465(7295):202–205.
41. Zadegan RM, et al. (2012) Construction of a 4 zeptoliters switchable 3D DNA box origami. *ACS Nano* 6(11):10050–10053.
42. Banerjee A, et al. (2013) Controlled release of encapsulated cargo from a DNA icosahedron using a chemical trigger. *Angew Chem Int Ed Engl* 52(27):6854–6857.
43. Numajiri K, Kimura M, Kuzuya A, Komiyama M (2010) Stepwise and reversible nanopatterning of proteins on a DNA origami scaffold. *Chem Commun (Camb)* 46(28):5127–5129.
44. Kuzuya A, Sakai Y, Yamazaki T, Xu Y, Komiyama M (2011) Nanomechanical DNA origami 'single-molecule beacons' directly imaged by atomic force microscopy. *Nat Commun* 2:449.
45. Han D, Pal S, Liu Y, Yan H (2010) Folding and cutting DNA into reconfigurable topological nanostructures. *Nat Nanotechnol* 5(10):712–717.
46. Kuzyk A, et al. (2014) Reconfigurable 3D plasmonic metamolecules. *Nat Mater* 13(9): 862–866.
47. Ding B, Seeman NC (2006) Operation of a DNA robot arm inserted into a 2D DNA crystalline substrate. *Science* 314(5805):1583–1585.
48. Lavella GJ, Jadhav AD, Maharbiz MM (2012) A synthetic chemomechanical machine driven by ligand-receptor bonding. *Nano Lett* 12(9):4983–4987.
49. Gu H, Yang W, Seeman NC (2010) DNA scissors device used to measure MutS binding to DNA mis-pairs. *J Am Chem Soc* 132(12):4352–4357.
50. Liu D, et al. (2006) A reversible pH-driven DNA nanoswitch array. *J Am Chem Soc* 128(6):2067–2071.
51. Liu D, Balasubramanian S (2003) A proton-fuelled DNA nanomachine. *Angew Chem Int Ed Engl* 42(46):5734–5736.
52. Shu W, et al. (2005) DNA molecular motor driven micromechanical cantilever arrays. *J Am Chem Soc* 127(48):17054–17060.
53. Li XM, Song J, Cheng T, Fu PY (2013) A duplex-triplex nucleic acid nanomachine that probes pH changes inside living cells during apoptosis. *Anal Bioanal Chem* 405(18):5993–5999.
54. Brucale M, Zuccheri G, Samorì B (2005) The dynamic properties of an intramolecular transition from DNA duplex to cytosine-thymine motif triplex. *Org Biomol Chem* 3(4): 575–577.
55. Aldaye FA, Sleiman HF (2007) Modular access to structurally switchable 3D discrete DNA assemblies. *J Am Chem Soc* 129(44):13376–13377.
56. Zhang Z, et al. (2011) A DNA tile actuator with eleven discrete states. *Angew Chem Int Ed Engl* 50(17):3983–3987.
57. Erdman AG, Sandor GN, Kota S (2001) *Mechanism Design: Analysis and Synthesis* (Prentice Hall, Upper Saddle River, NJ), 4th Ed.
58. Blanchoin L, et al. (2000) Direct observation of dendritic actin filament networks nucleated by Arp2/3 complex and WASP/Scar proteins. *Nature* 404(6781):1007–1011.
59. Bennett GT (1914) The skew isogram mechanism. *Proc London Math Soc 2* 13(1): 151–173.
60. Chen Y (2009) Design of structural mechanisms. PhD thesis (University of Oxford, Oxford).
61. Yu Y, Luo Y, Li L (2007) Deployable membrane structure based on the Bennett linkage. *Proc Inst Mech Eng Part G J Aerosp Eng* 221(5):775–783.
62. You Z, Chen Y (2011) *Motion Structures: Deployable Structural Assemblies of Mechanisms* (Taylor & Francis, Hoboken, NJ).
63. Bai XC, Martin TG, Scheres SH, Dietz H (2012) Cryo-EM structure of a 3D DNA-origami object. *Proc Natl Acad Sci USA* 109(49):20012–20017.
64. Kauert DJ, Kurth T, Liedl T, Seidel R (2011) Direct mechanical measurements reveal the material properties of three-dimensional DNA origami. *Nano Lett* 11(12):5558–5563.
65. Liedl T, Högberg B, Tytell J, Ingber DE, Shih WM (2010) Self-assembly of three-dimensional prestressed tensegrity structures from DNA. *Nat Nanotechnol* 5(7):520–524.
66. Zhou L, Marras AE, Su HJ, Castro CE (2014) DNA origami compliant nanostructures with tunable mechanical properties. *ACS Nano* 8(1):27–34.
67. Qian L, Winfree E, Bruck J (2011) Neural network computation with DNA strand displacement cascades. *Nature* 475(7356):368–372.
68. Zhang DY, Winfree E (2009) Control of DNA strand displacement kinetics using toehold exchange. *J Am Chem Soc* 131(47):17303–17314.
69. Seelig G, Soloveichik D, Zhang DY, Winfree E (2006) Enzyme-free nucleic acid logic circuits. *Science* 314(5805):1585–1588.
70. Douglas SM, et al. (2009) Rapid prototyping of 3D DNA-origami shapes with caDNAno. *Nucleic Acids Res* 37(15):5001–5006.